Acta Cryst. (1974). A30, 374

Low-Energy Electron Diffractometry from the Cleavage Face (001) of Magnesium Oxide

BY KAZUNOBU HAYAKAWA* AND SHIZUO MIYAKE†

Institute for Solid State Physics, University of Tokyo, Roppongi-7, Minatoku, Tokyo 106, *Japan*

(*Received* 19 *November* 1973; *accepted* 25 *December* 1973)

With a triple-axis low-energy electron diffractometer, the intensity curves of the specular reflexion 00 from the cleaved face (001) of a MgO crystal were measured against the glancing angle, for the electrons in the energy range from 180 eV to 500 eV and for three crystal azimuths in a range near [010]. By the use of diagrams drawn on the basis of the Ewald construction to indicate the surface wave resonance conditions for various reciprocal rods, a number of fine structures as well as gross features of the intensity curves were interpreted fairly well in terms of the resonance effect.

1. Introduction

The intensity curve of low-energy electron diffraction (LEED), obtained either by the variable-energy method or the constant-energy method, shows in most cases complicated features which require theoretical calculations of high approximation to interpret the details. Recent theoretical calculations, for instance those by Jepsen, Marcus & Jona (1972) and Pendry (1971*a*,*b*), succeeded fairly well in reproducing some examples of the intensity curves experimentally obtained. However, these calculations are not always suitable to give a ready physical understanding about the origin of individual anomalies in an intensity curve.

As a rule, an intensity curve of LEED, *e.g.* that obtained by the constant-energy method, changes sensitively with the variation of the electron energy and/or the crystal azimuth, and also extra peaks sometimes appear at off-Bragg positions. As pointed out in a previous paper (Miyake & Hayakawa, 1970), some of the anomalous behaviour in the LEED intensity curves can be ascribed to the 'resonance effect' [or Kikuchi–Nakagawa effect (Kikuchi & Nakagawa, 1933)]. This effect is a diffraction phenomenon in LEED which takes place when a Bragg reflexion (a surface wave) is excited in a direction parallel or nearly parallel to the crystal surface (McRae, 1966; McRae & Caldwell, 1967), and is essentially the same effect as Kikuchi & Nakagawa's anomaly known in HEED (Miyake & Hayakawa, 1970). As this effect may take place frequently in LEED, it is expected that the intensity curve in LEED may be affected by the resonance effect, not only partly but also with respect to the overall feature.

The present paper is concerned with the intensity measurement of the 00 reflexion from the cleavage surface (001) of the MgO crystal using the constant-energy method for various energies of the electrons, and the details of the intensity curves obtained were investigated with special reference to the resonance effect.

* Present address: Central Research Laboratory, Hitachi Ltd, Kokubunji, Tokyo 185, Japan.

† Home address: 2-29-1 Minami-Ogikubo, Suginami-ku, Tokyo 167, Japan.

2. Instrumental

In order to investigate the resonance effect in LEED, and also for more general purposes in LEED studies, a low-energy electron diffractometer with three rotating axes, as shown schematically in Fig. 1, was constructed. The radius of the fluorescent screen, made of surface-conductive glass, was 100 mm, the spacing between G_1 and G_2 was about 5 mm, and the receiving aperture of the Faraday cage was 4 mm ⌀.‡

‡ This apparatus can also be used for the electron diffraction experiments in the medium energy range of 1–5 keV (MEED).

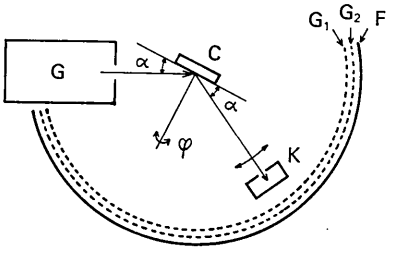

Fig. 1. Schematic diagram of a low-energy electron diffractometer. *G*, low-energy electron gun; *C*, crystal specimen; *K*, Faraday cage; G_1, G_2, cylindrical metal mesh electrodes; *F*, cylindrical fluorescent screen. α, glancing angle; φ, azimuthal angle.

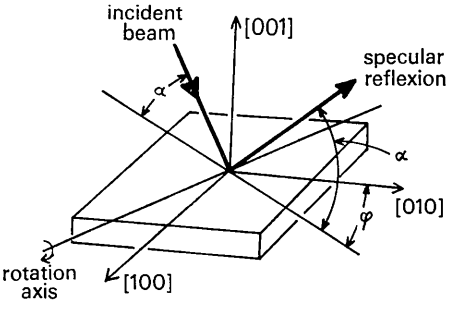

Fig. 2. Definition of the glancing angle α and the azimuthal angle φ.

The specimen crystal C and the Faraday cage K can be rotated either independently or in the α–2α relation around an axis perpendicular to the figure plane, where α is the glancing angle of the incident beam to the crystal surface. Rotation of these parts was operated from the outside of the vacuum. The smallest angular step of α was 0·05°. The azimuthal angle φ of the crystal was changed by rotating the specimen holder around an axis perpendicular to the crystal surface, and this angle was fixed as desired before each intensity measurement.

The diffractometer unit composed of these parts was enclosed in a vacuum chamber consisting of a glass bell-jar, which was connected to an ion sputtering pump. The operating pressure was in the range of 10^{-8} torr. This vacuum condition was enough to maintain the surface of MgO crystal free from contamination due to the electron irradiation.

3. Intensity measurement

The MgO specimen was prepared by cleaving a MgO single crystal in air. The area of the cleaved surface, about 10×20 mm, was sufficient to receive the whole beam even at the smallest range of the glancing angle. The intensity curve of the specular reflexion 00 was obtained as a function of the glancing angle α for various values of the electron energy E_p and the azimuthal angle φ. The glancing angle α and the azimuthal angle φ were defined as shown in Fig. 2. Each intensity measurement was performed by first setting the Faraday cage at the correct position to receive the specular reflexion, and then rotating the specimen and the Faraday cage together in the α–2α relation, over an angular range of α from 0 to 75°. The electron energy was changed every 40 eV step in the range from 180 to 500 eV. The crystal azimuths studied were:

A ([010]-azimuth): $\varphi = 0°$,
B: $\varphi = 5°$,
C: $\varphi = 10°$.

Fig. 3(a)–(c) shows the intensity curves thus obtained. The abscissa in each Figure is the glancing angle α and the ordinate is the reflected intensity normalized by the primary beam current which was of the order of 0·5 μA. The maximum current of the re-

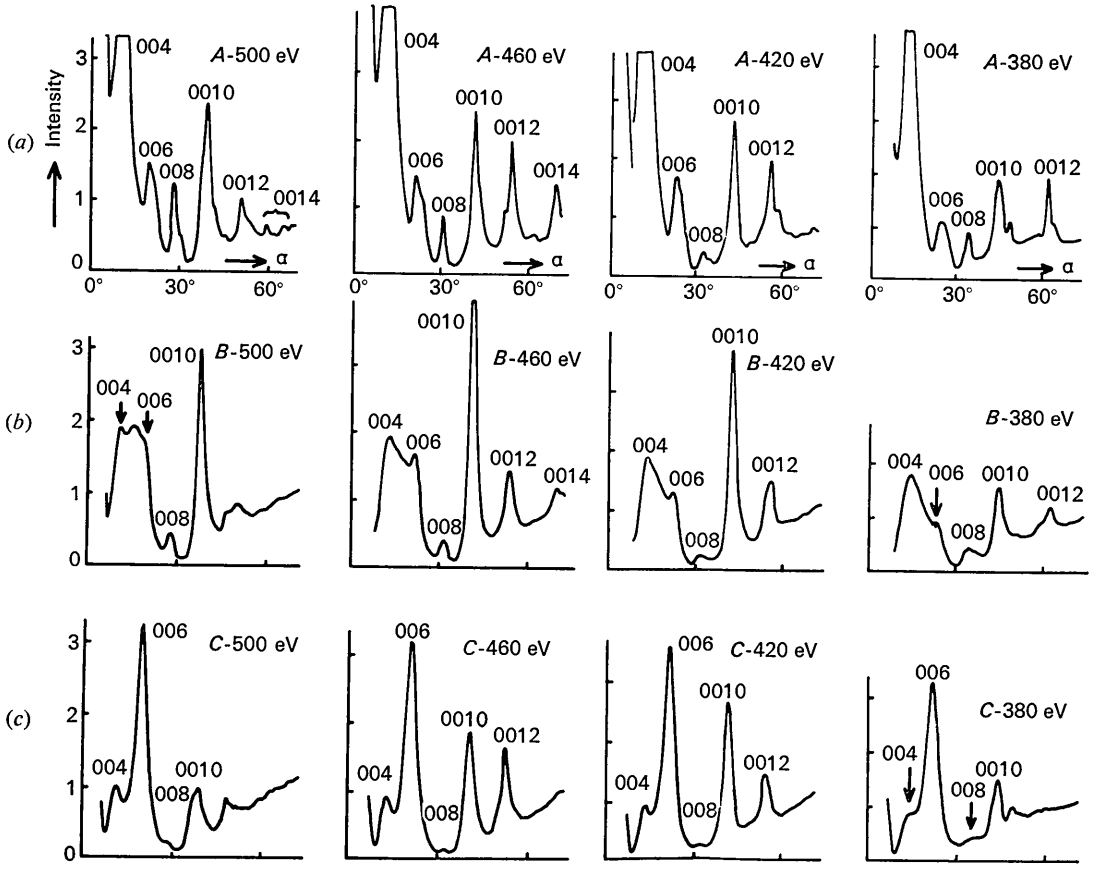

Fig. 3. Intensity curves of the specular reflexion for various electron energies E_p obtained from a MgO single-crystal cleavage surface. Abscissa: the glancing angle α, ordinate the reflexion intensity. Each interval between horizontal bars on the ordinates corresponds to the normalized intensity $2{\cdot}5 \times 10^{-3}$.

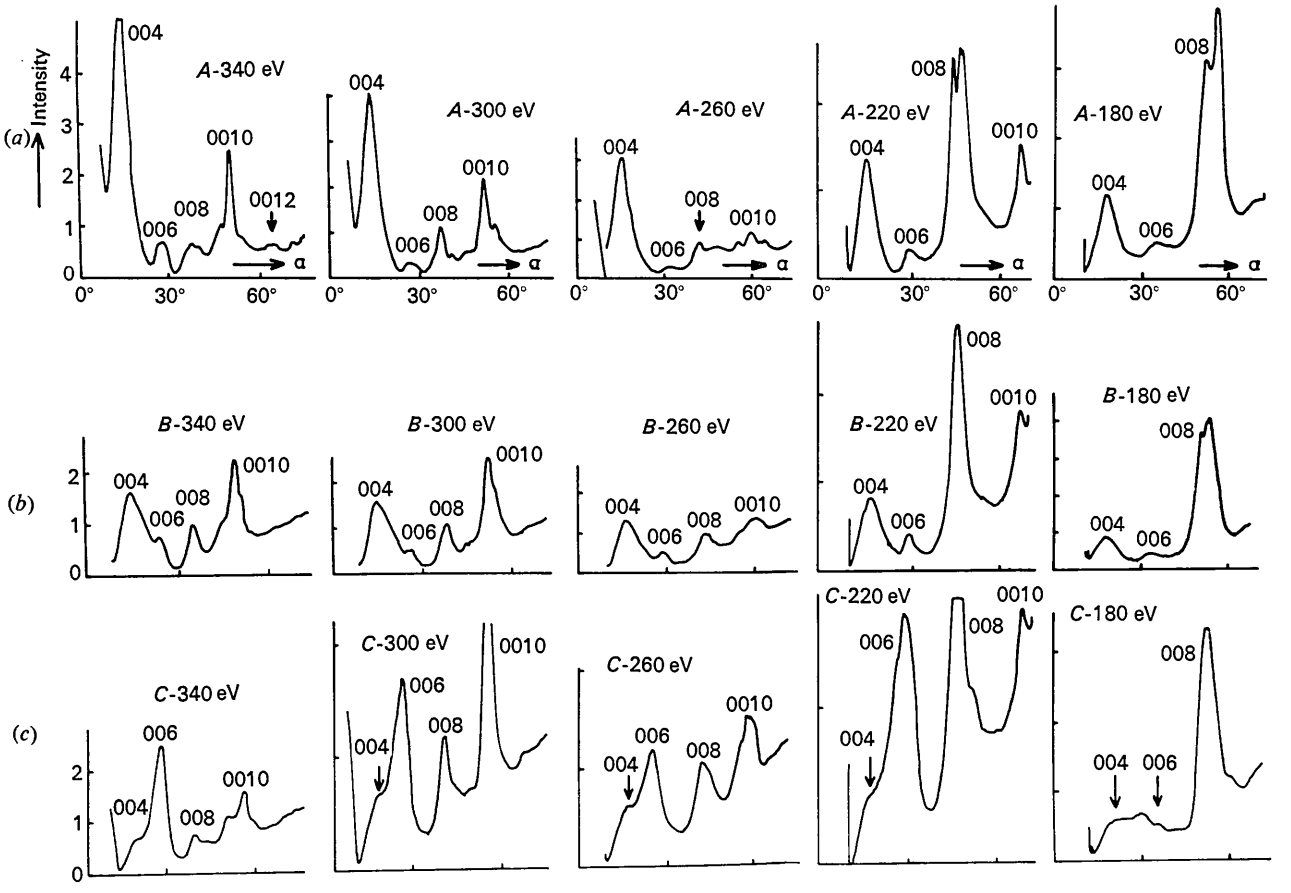

Fig. 3 (*cont.*)

flexion spot was of the order of 10^{-2} times the primary current. Hereafter, each curve in Fig. 3, *e.g.* that for the *A*-azimuth and 500 eV electrons, is designated as *A*-500 eV.

In addition to the intensity measurement described above, visual and photographic pattern observations were performed. The pattern observation was useful in giving the relation between the intensity behaviour of the 00 spot and the overall feature of the diffraction pattern. Figs. 4–8 are examples of the photographic patterns, which were obtained at the glancing angles indicated in each of the accompanying intensity curves.

4. Resonance condition

(*a*) *Ewald construction*

The resonance effect takes place when a diffracted beam is excited in a direction parallel or nearly parallel to the crystal surface. This condition can be obtained by the Ewald construction, as follows.

When, for instance, the specular reflexion 00 satisfies the Bragg condition 004 for a given incident beam in the [010] azimuth (*A*-azimuth), the surface waves 202 and $\bar{2}02$ are additionally excited since the reciprocal-lattice points 202 and $\bar{2}02$ come to lie on the horizontal great circle of the Ewald sphere. In this case, the reciprocal rods 20 and $\bar{2}0$ are tangential to the Ewald sphere at the points 202 and $\bar{2}02$. In other words, these vertical rods intersect perpendicularly the horizontal great circle which is in the plane parallel to the crystal surface (001) and passing through the centre of the sphere *A*, as shown in Fig. 9. We may say that, under the assumed condition both the 20-rod resonance and the $\bar{2}0$-rod resonance take place simultaneously with the 004 Bragg reflexion.

As illustrated by the above example, the resonance condition, or the condition for each rod resonance, can generally be obtained by finding out the condition that a vertical reciprocal-lattice rod intersects the horizontal great circle of the Ewald sphere. Fig. 10 shows this circle and the intersecting points with the figure plane of the vertical rod array for the MgO crystal with the cleavage surface (001). The radius of the Ewald sphere and, accordingly that of the horizontal great circle, is assumed to be $\kappa_0 = n_0 K$, where $K = 1/\lambda$, λ is the electron wavelength in free space, n_0 is the mean refractive index of the crystal for the electrons and is equal to $(1 + eV_0/E_p)^{1/2}$, where E_p is the electron energy, V_0 is the

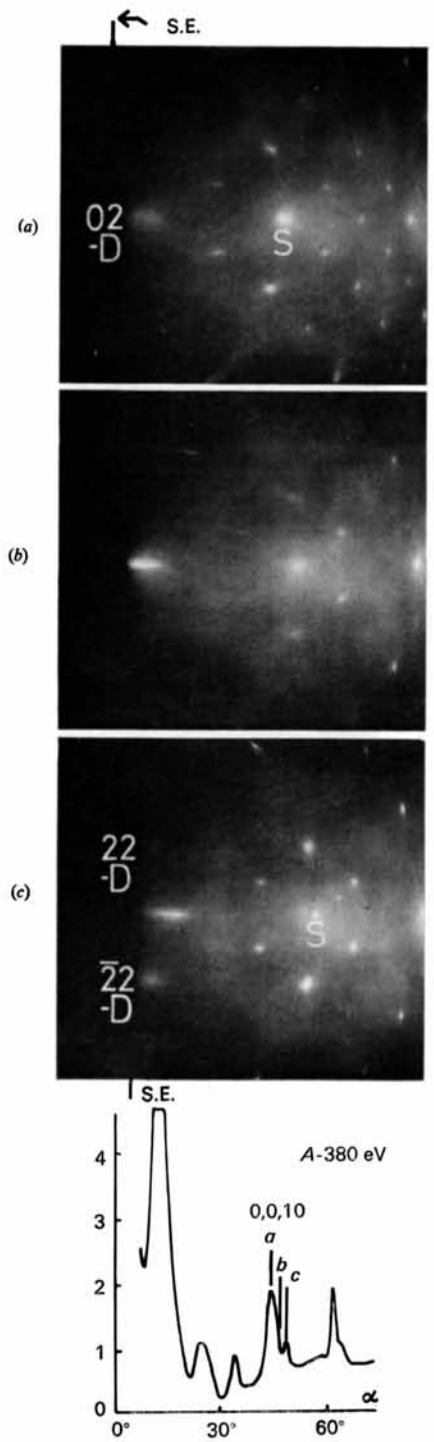

Fig. 4. Diffraction patterns in which the specular reflexion S is nearly at the condition of 0,0,10 peak in A-380 eV. S.E.: the shadow edge. The 02-rod resonance takes place in the vicinity of (a), in which the 02 diffuse spot (02-D) begins to appear above the shadow edge. The $\bar{2}2$-rod resonance takes place at (c), in which the $\bar{2}2$-diffuse spot ($\bar{2}2$-D) is observed.

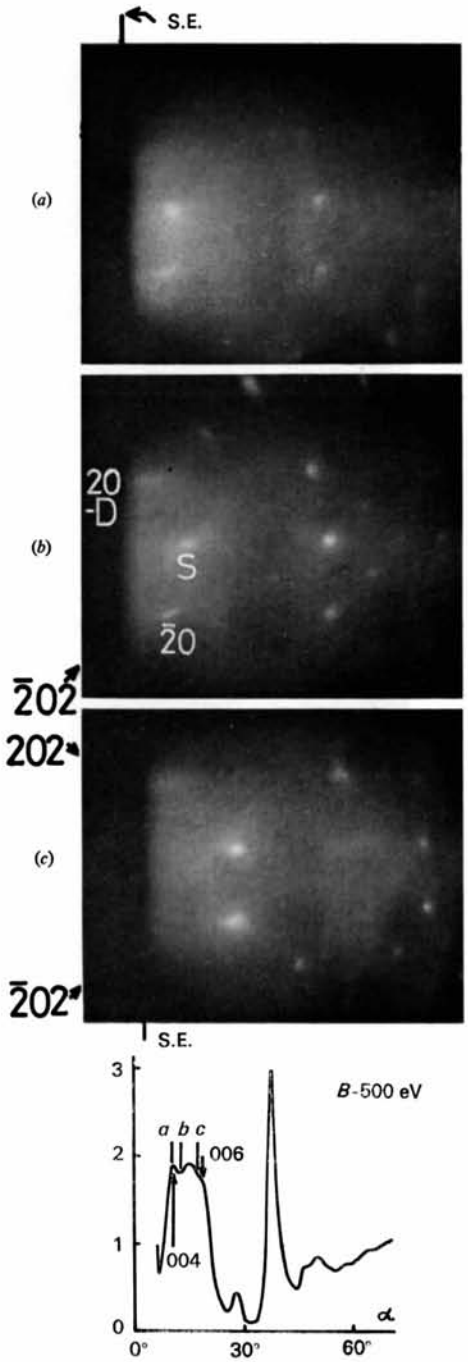

Fig. 5. Diffraction patterns in the range of the lowest order peak in B-500 eV. The 20-rod resonance condition is satisfied in the vicinity of (b), in which the specular reflexion S lies on the Kikuchi line $\bar{2}02$ and also a diffuse spot (20-D) belonging to the 20 rod begins to appear.

[To face p. 376

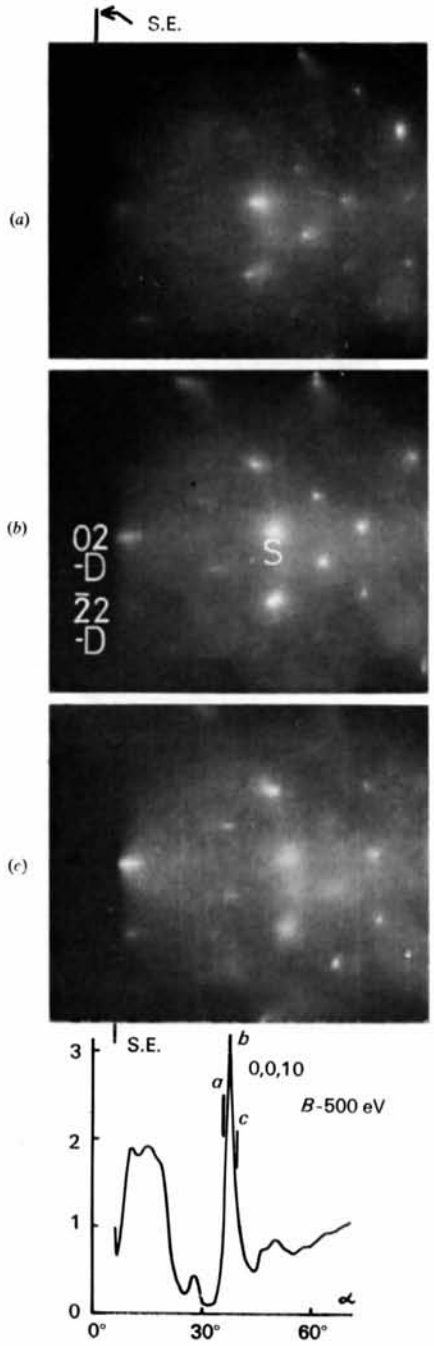

Fig. 6. Diffraction patterns in *B*-500 eV. S.E.; the shadow edge The specular reflexion *S* in the range of the Bragg condition 0,0,10 is enhanced by the 02-rod resonance. The 02-rod diffuse spot (02-*D*) is observed at the shadow edge in (*b*). Successive occurrence of the 02- and $\bar{2}2$-rod resonances can be known from the appearance of the corresponding diffuse spots by a slight change of the glancing angle.

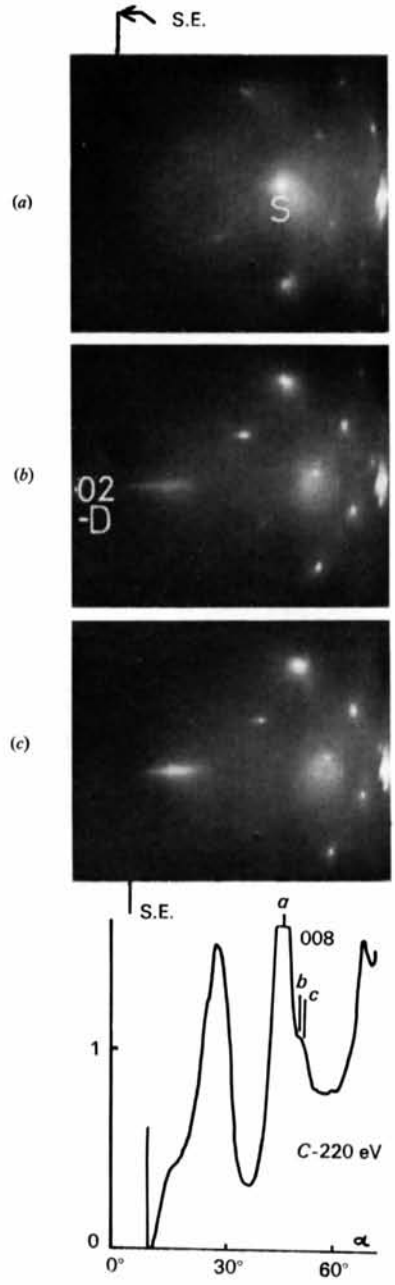

Fig. 7. Diffraction patterns in *C*-220 eV. The specular reflexion *S* satisfying the Bragg condition 008 is remarkably enhanced in (*a*) and, correspondingly, the appearance of the 02-rod diffuse spot (02-*D*) is observed in (*b*), showing that the intensity enhancement of *S* is due to the 02-rod resonance.

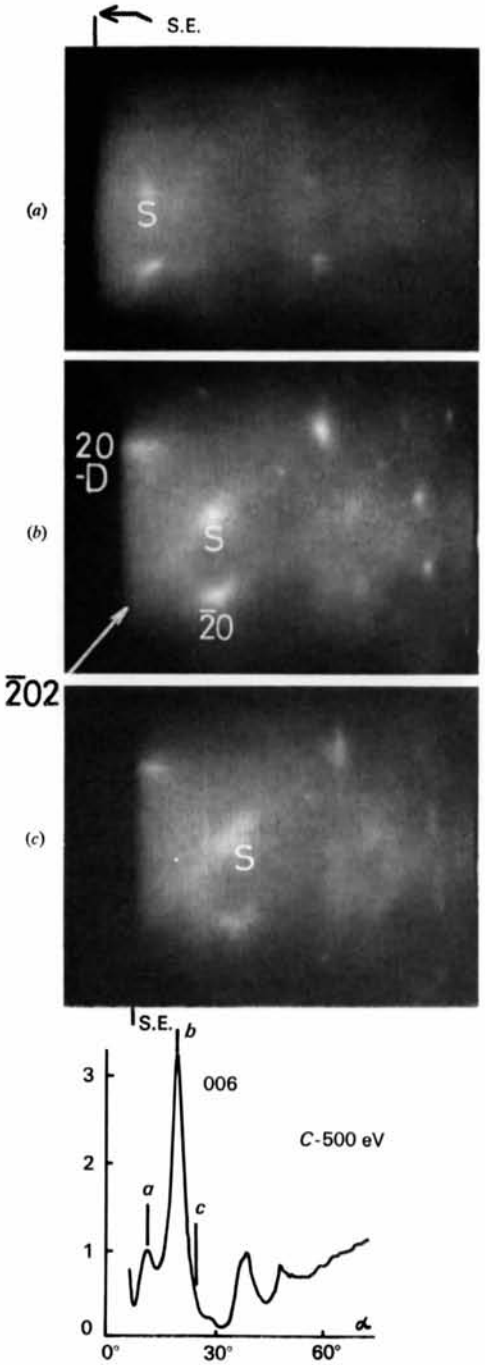

Fig. 8. Diffraction patterns in C-500 eV. In (b) the Kikuchi line $\bar{2}02$ passes through the spot S and the 20-rod diffuse spot is simultaneously observed, indicating that the intensity of the specular reflexion satisfying the Bragg condition 006 is enhanced by the 20-rod resonance. It should also be noticed that the intensity of each diffraction spot is abruptly weakened in the photograph (c).

mean inner potential and e is the electron charge.* The centre of the great circle, A, is determined by the indent beam in a given azimuth φ, and $AO=K\cos\alpha=\kappa_0\cos\alpha'$, where α is the glancing angle of the incident electrons and α' that of the refracted primary beam in the crystal. The point A moves with the change of α. Fig. 10 explains that the 20-rod resonance, for example, is realized when the centre of the great circle comes at the position A'.

By this kind of consideration, we can determine the resonance conditions for various lattice rods. The results thus obtained are indicated by the curves shown in Fig. 11(*a*)–(*c*). From these curves, the condition for each rod resonance is known in terms of E_p+eV_0 given in the ordinate and of the value of $2a_0\kappa_0\sin\alpha'$ given in the abscissa, where a_0 is the edge length of the cubic unit cell. Hereafter, we call each curve the 'resonance curve'. The vertical lines marked by integers l on the abscissae in Fig. 11(*a*)–(*c*) correspond to the calculated Bragg conditions for 00l including the refraction effect.

As already pointed out, the Bragg condition 004 in the A azimuth always coincides with the resonance conditions for the 20 and $\bar{2}0$ rods. Similarly, the Bragg condition for 008 in the same azimuth coincides with the resonance conditions for the 40 and $\bar{4}0$ rods. Therefore, in the A azimuth the resonance curves for these rods are given by the vertical straight lines, as shown in Fig. 11(*a*). However, the other resonance curves in the same figure are oblique curves. In the B and C azimuths, the resonance curves are all oblique curves, as shown in Fig. 11(*b*)–(*c*).

It is noted that the 02- and 04-rod resonance curves are almost independent of the crystal azimuth, while the other curves change their forms and location considerably with the azimuth.

* In this paper the resonance condition is defined as that given by the Ewald construction using the sphere with a radius equal to the wave number in the crystal.

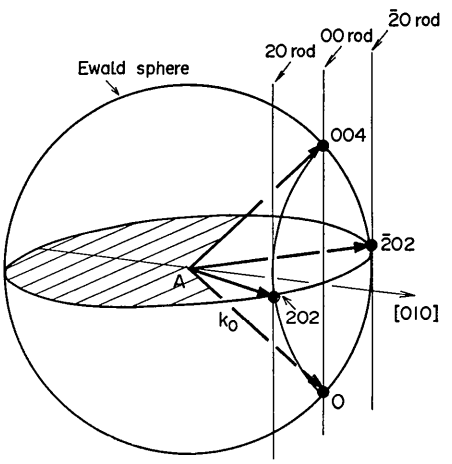

Fig. 9. Ewald construction for the incident beam satisfying 004 in the A([010]) azimuth.

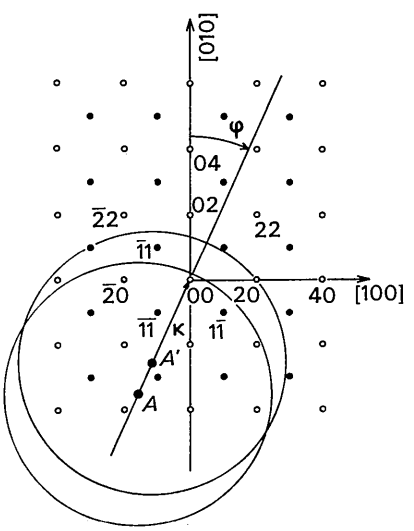

Fig. 10. Movement of the horizontal great circle of the Ewald sphere, and the reciprocal-rod array perpendicular to the cleavage face (001) of MgO. κ_0 (radius of the horizontal great circles): the mean wave number in the crystal. A, A': the centres of the horizontal great circles. Open circles, even-order rods; filled dots; odd-order rods.

(*b*) *Experimental methods*

There are also experimental methods for obtaining the resonance condition. One method is based on the fact that the coincidence of the specular reflexion with a Kikuchi line corresponds to a resonance condition (Miyake, Kohra & Takagi, 1954; Miyake & Hayakawa, 1970). However, this method which is quite useful in HEED is not so powerful in LEED, mainly because Kikuchi patterns are distinctly visible only in the energy range higher than about 300 eV (see Figs. 4–8).

Another method involves observing the thermal diffuse spot (Hayakawa, 1968). If the glancing angle α is increased from a value corresponding to the condition of the hk-rod resonance, then a diffraction spot hkl belonging to the same rod begins to appear above the shadow edge. What first appears in this process is the thermal diffuse spot accompanying the hkl reflexion, and this spot can be readily identified by its characteristic features; it is apparently diffuse and considerably elongated in the direction perpendicular to the shadow edge owing to the refraction effect, as seen in Figs. 4–8. If, therefore, we observe the rise of a thermal diffuse spot above the shadow edge at a glancing angle α_d, we can conclude that a resonance condition takes place almost simultaneously at this angle, or has been realized at a value of α slightly smaller than α_d. This kind of observation was practically fruitful in confirming the considerations based on the Ewald construction.

5. Interpretation of the intensity curves

In the present section it is shown by some typical examples that important features of the intensity curves in Fig. 3 may be understood in terms of the resonance curves in Fig. 11.

(a) Fine structures

Fig. 12 illustrates an example in which a fairly complicated fine structure of an intensity curve can be interpreted as a group of intensity peaks corresponding to a number of rod resonances. Fig. 12(*a*) is a part of the intensity curve *A*-260 eV in Fig. 3, and (*b*) corresponds to the relevant part of Fig. 11(*a*), drawn as a function of α assuming the mean inner potential to be $V_0 = 14$ V. By comparison of the two Figures, it is evident that the peak *a* is the 008 Bragg reflexion affected by the simultaneous resonances for the 40 and $\bar{4}0$ rods, the peak *d* is the 0,0,10 Bragg reflexion, and the peaks *b*, *c* and *e* are no doubt the extra intensity maxima corresponding to the 02-rod, 22-rod + $\bar{2}2$-rod, and 42-rod + $\bar{4}2$-rod resonances, respectively. Although there are some discrepancies between the peak positions and the resonance conditions given by the resonance curves, the correspondence between them can be confirmed by inspecting the systematic change of the intensity curve with the electron energy. Most fine structures found in the intensity curves for the *A* azimuth can be explained in the similar way. Fig. 13 is another example, where (*a*) is a part of *A*-380 eV in Fig. 3 and (*b*) corresponds to the relevant part of Fig. 11(*a*). It is noted that there is a close coupling between the Bragg reflexion 0,0,10 and the 02-, $\bar{2}2$- and 22-rod resonances (*cf.* Fig. 4).

A similar analysis is also applicable to the intensity curves for the *B* and *C* azimuths. Fig. 14 is concerned with the fine structure of the lowest order peak in the intensity curve *B*-500 eV in Fig. 3. This peak is found to be a combination of the 004 and 006 Bragg reflexions and the peak due to the 20-rod resonance (*cf.* Fig. 5). In this connexion, it is interesting to note that the peak profile in this case is quite similar to that of the lowest-order peak in the intensity curve *C*-180 eV except for the difference in the peak height. This similarity is well understood from Fig. 11, which shows that the mutual relation among the Bragg conditions 004, 006 and the condition of the 20-rod resonance is similar for *B*-500 eV and *C*-180 eV. In these cases, the $\bar{4}0$-rod resonance seems to be not so influential.

The intensity curves in the *B* and *C* azimuths are generally flatter and have less fine structure than those in the *A* azimuth. This is probably because the resonance curves in the *B* and *C* azimuths are more crowded than those in the *A* azimuth.

(b) Remarkable enhancement of the peak intensities

In the intensity curves shown in Fig. 3, there are a number of extraordinarily enchanced peaks, such as the 004 peak in the *A* azimuth, the 0,0,10 in *B*-460 eV and in *C*-300 eV and the 008 peak in *C*-220 eV. These remarkable peaks can be interpreted as follows.

The 004 peak in the *A* azimuth is enhanced by simultaneous participation of the 20- and $\bar{2}0$-rod resonances which involve the surface waves 202 and $\bar{2}02$ belonging to these rods. This effect is especially conspicuous in the energy range from 500 to 340 eV. How-

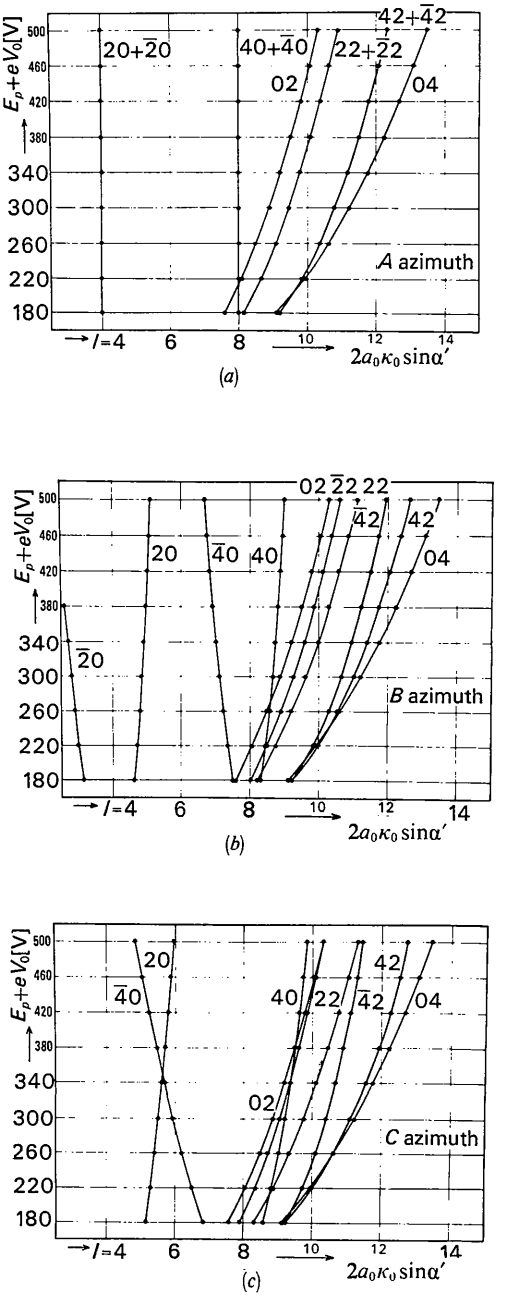

Fig. 11.(*a*), (*b*), (*c*) Calculated resonance curves for *A*, *B* and *C* azimuths. The ordinate is $E_0 + eV_0$ and the abscissa, $2a_0\kappa_0 \sin\alpha'$, κ_0 and α' are the mean wave number and the glancing angle in the crystal respectively (see the text). Indices '20', for instance, indicate the resonance curve for the 20-rod resonance.

ever, this peak becomes less marked below 340 eV. This seems to suggest that the 202 and $\bar{2}02$ surface waves are gradually extinguished as the electron energy decreases.

The remarkable intensity of the 0,0,10 peak in *B*-460 eV is apparently due to the coincidence of the Bragg condition 0,0,10 with the 02-rod resonance, as indicated by the 02 resonance curve in Fig. 11(*b*) (*cf.* Fig. 6 for *B*-500 eV). Similarly, the strong peak 0,0,10 in *C*-300 eV can be ascribed to the coincidence with the 22-rod resonance. The strong peak of 008 in *C*-220 eV is also in coincidence with the 02-rod resonance (*cf.* Fig. 7). The fairly strong intensities of the 008 peak in *C*-180 eV, *A*-220–180 eV and *B*-220–180 eV may also be ascribed to the same situation.

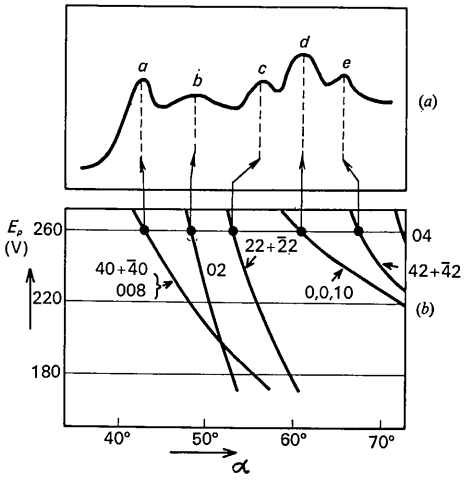

Fig. 12. (*a*) Fine structure in the intensity curve of *A*-260 eV. (*b*) A part of Fig. 11(*a*) converted to a function of α, assuming the mean inner potential $V_0 = 14$ V.

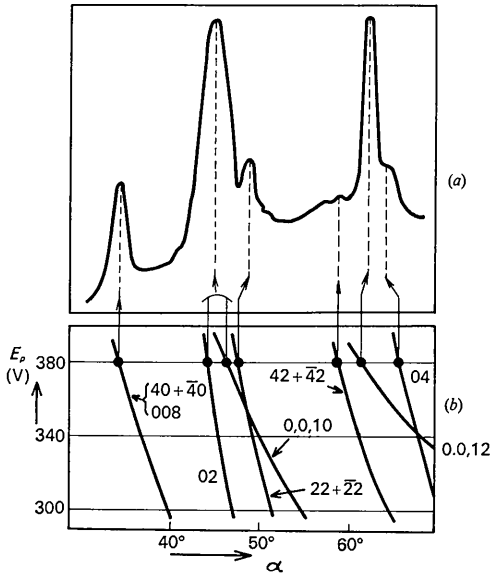

Fig. 13. (*a*) Part of *A*-380 eV. (*b*) Part of Fig. 11(*a*) converted to a function of α. ($V_0 = 14$V).

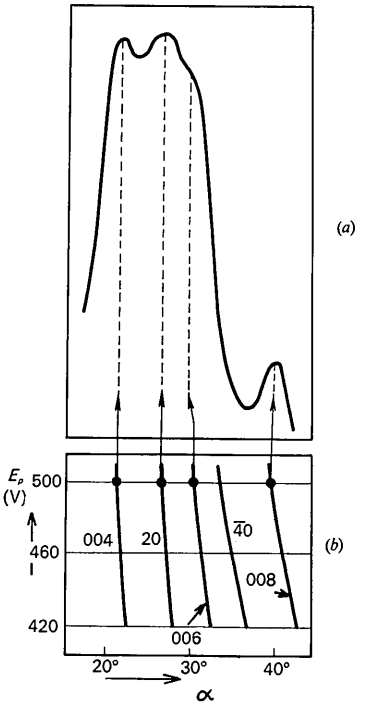

Fig. 14. (*a*) Part of *B*-500 eV. (*b*) Part of Fig. 11(*b*) converted to a function of α. ($V_0 = 14$V).

It is also noted in *B*-220 eV and *C*-220 eV that the 0,0,10 peak is enhanced by the 04-rod resonance.

(*c*) *Reflexion intensity at the off-resonance condition*

Although, as described above, the 004 peak is exceedingly strong in the *A* azimuth, it is not so significant in the *B* azimuth, being comparable with the 006 peak. This abrupt change occurs because the simultaneous condition for the Bragg reflexion 004 and for the 20- and $\bar{2}$0-rod resonances is lost in the *B* azimuth.

The 004 peak is depressed still further in the *C* azimuth. On the contrary, the 006 peak which is not so conspicuous in the *A* and *B* azimuths becomes remarkable in the *C* azimuth (*cf.* Fig. 8). This feature can be understood from the behaviour of the 20-rod resonance curve in Fig. 11(*c*), which runs very close to the vertical line corresponding to the Bragg reflexion 006 over a wide range of electron energy (*cf.* Fig. 8). On the other hand, it is noticeable in the same Figure that there is no resonance curve in the vicinity of the vertical line corresponding to the 004 Bragg condition.

It is the general trend that a Bragg reflexion which is not accompanied by any rod resonance is rather weak. The weak intensities of the 008 peak in *B*-500–300 eV correspond to a similar case.

6. Discussion

As known from a number of examples in §5(*b*)–(*c*), most of Bragg peaks with appreciable intensities are those which are more or less affected by the existence

of resonance effects. The resonance effect possesses, so to speak, a 'pumping action', by which the waves propagating into the crystal are efficiently converted to outgoing waves. As was calculated for HEED by Kohra, Molière, Nakano & Ariyama (1962), the reflectivity of the specular reflexion enhanced by a resonance effect may nearly attain unity in the non-absorbing case. The pumping action of the resonance effect is very important for the understanding of LEED phenomena in general, since resonance takes place more frequently in LEED than in HEED, mainly because of the small radius of the Ewald sphere in the former case. Consider, for instance, the experimental condition of normal incidence of the electrons at the crystal surface. In this case, the electron scattering in forward directions may efficiently be converted to the backward scattering with scattering angle about 180° through the resonance effect, provided that the effective value of the atomic scattering factor for the 90° scattering is more or less appreciable, even if that for the direct 180° scattering is not so.

In the present paper, it has been shown that some fine structures as well as gross features of the intensity curves can be qualitatively interpreted fairly well in terms of the resonance effect. Naturally, the present method of analysis is difficult to take over into quantitative interpretation. However, by the present method, it is possible to know which rod resonances have a particular influence on the reflexion intensity in a limited range of electron energy and glancing angle. It is conceived that such information may be used as a guide for theoretical work in order to set up an appropriate approximation in individual cases.

References

HAYAKAWA, K. (1968). *J. Phys. Soc. Japan*, **25**, 1647–1653.

JEPSEN, D. W., MARCUS, P. M. & JONA, F. (1972) *Phys. Rev.* B**6**, 3684–3690.

KIKUCHI, S. & NAKAGAWA, S. (1933). *Sci. Pap. Inst. Phys. Chem. Res. Tokyo*, **21**, 256–265.

KOHRA, K., MOLIÈRE, K., NAKANO, S. & ARIYAMA, M. (1962). *J. Phys. Soc. Japan*, **17**, Supp.I B-II, 82–84.

MCRAE, E. G. (1966). *J. Chem. Phys.* **45**, 3258–3276.

MCRAE, E. G. & CALDWELL, C. W. (1967). *Surf. Sci.* **7**, 41–67.

MIYAKE, S. & HAYAKAWA, K. (1970). *Acta Cryst.* A**26**, 60–70.

MIYAKE, S., KOHRA, K. & TAKAGI, M. (1954). *Acta Cryst.* **7**, 393–401.

PENDRY, J. B. (1971*a*). *J. Phys.* C**4**, 2501–2513, 2514–2523.

PENDRY, J. B. (1971*b*). *J. Phys.* C**4**, 3095–3106.

Acta Cryst. (1974). A**30**, 380

Magnetische Struktur des Trirutils $FeTa_2O_6$

VON HANS WEITZEL UND SIEGFRIED KLEIN

Fachgebiet Strukturforschung der TH, D 61 *Darmstadt, Deutschland (BRD)*

(*Eingegangen am* 25. *Oktober* 1973; *angenommen am* 6. *Dezember* 1973)

By means of neutron diffraction the magnetic structure of $FeTa_2O_6$ has been determined. The observed magnetic reflexions define a unit cell $2a$, b, $2c$. In order to match the tetragonal symmetry this cell must be enlarged again, which results in the final magnetic cell $2a$, $2b$, $2c$ with the magnetic space group $Ic4_1/a$. The structure contains two sublattices with the cells $2a$, b, $2c$ and a, $2b$, $2c$, the moments of which are perpendicular to each other. The moments lie in the a/b plane and form an angle of $\varphi_a = 45°$ with the a axis. The spin quantum number is found to be $S = 2{\cdot}04$.

Einleitung

Von Trirutilen AB_2O_6 mit dem magnetischen Kation auf dem A-Platz sind noch keine magnetischen Strukturen bestimmt worden. Bekannt ist aufgrund von Neutronenbeugungsmessungen lediglich, dass die Substanz $NiTa_2O_6$ eine komplizierte magnetische Struktur besitzt, ohne dass die Struktur jedoch bisher gelöst werden konnte (Kunnmann, La Placa, Corliss, Hastings & Banks, 1968). Im folgenden soll über die Bestimmung der magnetischen Struktur des Trirutils $FeTa_2O_6$ aus einem Neutronenbeugungspulverdiagramm berichtet werden. Wohl konnten mit Neutronenbeugung die magnetischen Strukturen von inversen Trirutilen gefunden werden, nämlich von Cr_2WO_6 (Kunnmann *et al.*, 1968; Montmory & Newnham, 1968), Cr_2TeO_6 (Kunnmann *et al.*, 1968; Montmory & Newnham, 1968), Fe_2TeO_6 (Kunnmann *et al.*, 1968; Montmory, Belakhovsky, Chevalier & Newnham, 1968) und V_2WO_6 (Kunnmann *et al.*, 1968). In letzter Zeit ist noch die magnetische Struktur von $LiFe_2F_6$ hinzugekommen (Shachar, Makovsky & Shaked, 1972; Wintenberger, Tressaud & Menil, 1972). In diesen inversen Trirutilen besetzen die magnetischen Kationen den B-Platz, so dass die magnetischen Strukturtypen sich wesentlich von denen der Trirutile unterscheiden müssen. Dagegen sind die bei den Trirutilen zu erwartenden magnetischen Strukturtypen